Development and characterization of yttria stabilized zirconia and Al2O3 thin films by pulsed laser deposition: Special Issue

Nath, S, Manna, I, Ray, SK & Dutta Majumdar, J

Original citation & hyperlink:
Nath, S, Manna, I, Ray, SK & Dutta Majumdar, J 2016, 'Development and characterization of yttria stabilized zirconia and Al2O3 thin films by pulsed laser deposition: Special Issue' *Lasers in Engineering*, vol 35, no. 1-4, pp. 101-122
http://www.oldcitypublishing.com/journals/lie-home/lie-issue-contents/lie-volume-35-number-1-4-2016/lie-35-1-4-p-101-122/

ISSN 0898-1507
ESSN 1029-029X

Publisher: Old City Publishing

Development and Characterization of Yttria Stabilized Zirconia and Al_2O_3 Thin Film by Pulsed Laser Deposition

Subhasisa Nath[a, 1], Indranil Manna[a, c, 2], Samit Kumar Ray[b, 3] and Jyotsna Dutta Majumdar[a, 4,*]

[a] *Department of Metallurgical & Materials Engineering, Indian Institute of Technology, Kharagpur, West Bengal*
[b] *Department of Physics, Indian Institute of Technology, Kharagpur, West Bengal*
[c] *Indian Institute of Technology, Kanpur, Uttar Pradesh*
[1]sendsubha@gmail.com; [2]imanna@metal.iitkgp.ernet.in;
[3]physkr@phy.iitkgp.ernet.in; [4]jyotsna@metal.iitkgp.ernet.in

ABSTRACT

The present study concerns development of yttria stabilized zirconia (YSZ), Al_2O_3 and a multilayer of Al_2O_3-YSZ thin film deposition by pulsed laser deposition (PLD) technique for its application as thermal barrier coating (TBC). The detailed study included characterization (microstructure, composition, phase and surface topography) of the thin film. The phase analysis of the YSZ films deposited at room temperature showed amorphous feature, while the film deposited at high temperature showed the formation of tetragonal phase. Residual stress analysis of the coating showed the presence of compressive stress and was maximum at 573 K (σ_{11} = -8.1 GPa and σ_{22} = -6.4 GPa). Residual stress was found to decease with increase in substrate temperature and was found to be lowest at 973 K (σ_{11} = -3.0 GPa and σ_{22} = -1.7 GPa). The cross-sectional morphology of the YSZ and Al_2O_3 thin films deposited at room temperature showed presence of inter-columnar porosities which changed to a dense structure with increase in substrate temperature.

Keywords: *KrF excimer laser, yttria stabilized zirconia (YSZ), Al_2O_3, alumina, thin film, thermal barrier coating (TBC), pulsed laser deposition (PLD), microstructure, residual stress*

*Corresponding author FAX: +91-3222-282280

1. INTRODUCTION

Ceramic materials have been used as structural material for wide range of applications. Yttria stabilized zirconia (YSZ) found its application in aviation and power generation industries as materials for thermal barrier coating [1]. Apart from being used as a thermal barrier material, it has found its application for the components against wear because of its high hardness and chemical inertness [2]. YSZ has been used as protective coatings against high temperature oxidation due to its low thermal conductivity and thermo-mechanical compatibility with the underlying substrate [3]. YSZ has also been used as an electrolyte material for Solid Oxide Fuel Cell (SOFC) due to its high ionic conductivity, chemically inertness and stability at high temperature [4]. Yttria (3-8 mol. %) has been used as a dopant to stabilize the high temperature tetragonal phase of zirconia at room temperature. Addition of Y_2O_3 to ZrO_2 produces oxygen vacancies in the crystal which accounts for increase in the ionic conductivity of the material. Stabilization of tetragonal phase to room temperature results in excellent thermal shock resistance and thereby, increasing the lifetime of the component operating in harsh environment [5]. Aluminium oxide (Al_2O_3) has also been used for many structural applications because of its high melting point, high hardness, superior wear resistance and corrosion resistance. Alumina exists in several polymorphs out of which α phase is the most thermodynamically stable one whereas, phases like γ, θ, κ are metastable in nature [6, 7]. Alumina thin films have also been used for the oxygen diffusion barrier device applications [8] as well as for oxidation protection in thermal barrier coatings [9-11]. Al_2O_3 coatings have been deposited by chemical vapour deposition (CVD) technique, sol-gel technique, DC magnetron sputtering, electron beam evaporation, plasma spraying (PS), spray pyrolysis, and pulsed laser deposition (PLD) techniques [12]. Among the above mentioned deposition methods, PLD technique has been

found to be the most suitable deposition method for obtaining dense multicomponent films with stoichiometric composition as that of target.

PLD technique involves irradiation of single or multiple targets by a pulsed laser beam which results in melting, evaporation and ionization of species and formation of high density plasma plume made up of ablation species. The formation of plasma plume is followed by an adiabatic expansion of plasma plume away from the target surface or towards the substrate where, the ablation species are condensed, followed by formation of films on the substrate. Substrate temperature can be varied to change the diffusion and kinetic energy of the ablated species on the surface of substrate [13, 14]. PLD technique has been found to be the most suitable deposition method for obtaining dense multicomponent films with stoichiometric composition as that of target. The structure, morphology and hence, properties are mainly affected by the deposition parameters (such as substrate temperature, oxygen pressure, substrate-target distance etc.) in PLD method [15, 16]. In the past, several studies have been carried out in for the evaluation of structural, optical, electrical, and mechanical properties of pulsed laser deposited YSZ, and Al_2O_3 thin films [16-26]. Pulsed laser deposition has also been used for the development of nano-structured thin films [27, 28].

In the present study, pulsed laser deposition of YSZ, Al_2O_3 and a multilayer of YSZ and Al_2O_3 thin films has been carried out. Followed by deposition, a detailed characterization of surface topography, microstructure and phases have been undertaken.

2. EXPERIMENTAL

2.1. Materials

A 7 wt% Yittria stabilized zirconia (7YSZ) powder (99.95% purity) and alumina (Al_2O_3) powder (99.95% purity) were compacted using an applied pressure of 10 ton and sintered in air at 1600 °C for 6 hours to prepare targets in the form of pellets (dia. 25 mm) to be used for pulsed laser deposition. Figure 1 shows the X-ray diffraction (XRD) patterns of the 7YSZ precursor powder (plot 1) and sintered pellet (plot 2) used for pulsed laser deposition. From plot 1, it can be seen that the YSZ powder contains mixture of tetragonal zirconia (t -ZrO_2) and monoclinic zirconia (m -ZrO_2) phases**.** However, YSZ sintered pellet (plot 2) was found to contain the tetragonal zirconia phase as major phase with a few monoclinic zirconia phases. The volume fraction of monoclinic and tetragonal phase in precursor YSZ powder and YSZ pellet was measured by the method proposed by Miller *et al* [29]. Table 1 shows the volume fraction of monoclinic and tetragonal phase in YSZ powder and pellet. From Table 1, it can be seen that the volume fractions of monoclinic and tetragonal phase in the precursor powder are 29.1% and 70.9%, respectively. On the other hand, for YSZ sintered pellet, the volume fraction of monoclinic and tetragonal phase was found to 2.6% and 97.4%, respectively. Table 1 summarizes the crystallite size and lattice strain present in as-received YSZ powder and sintered YSZ pellet used in the present study. From Table 1, it may be noted that there is no significant difference in crystallite size between as-received YSZ powder and sintered YSZ pellet. Furthermore, the lattice strain for monoclinic phase is found to be higher in YSZ pellet than YSZ powder which may be attributed to the transformation of monoclinic phase to tetragonal phase due to heat treatment (cf. Table 1). Figure 2 shows the XRD patterns of alumina precursor powder (plot 1) and sintered pellet (plot 2) used for pulsed laser deposition. From plot 1 and plot 2, it can be noted that α-Al_2O_3 was the major phase in both precursor powder and sintered pellet and there is no separate phase formation due to compaction followed by sintering. The details of

crystallite size and lattice strain of α-Al_2O_3 phase in as-received powder and sintered pellet has been summarized in Table 1. From Table 1, it may be noted that the crystallite size in as-received powder was found to be 97 nm whereas in sintered pellet the crystallite size was found to be 127 nm. Furthermore, the lattice strain for α-Al_2O_3 phase in as-received powder was found to be 0.12% as compared to 0.08 % in sintered pellet. Hence, it may be concluded that there is a marginal change in lattice strain due to sintering. However, the increase in crystallite size may be attributed to the grain growth due to heat treatment. Figure 3 shows the FESEM micrographs of (a) YSZ (b) Al_2O_3 precursor powders used for the preparation of targets for pulsed laser deposition. From Figure 3a, it can be seen that the particles of YSZ are spherical in shape with particle size ranging from 15 μm to 85 μm. Furthermore, the powders are porous in nature. However, the shapes of Al_2O_3 precursor powders are angular in nature with particle size ranging from 22 μm to 45 μm. The substrates used for the pulsed laser deposition were Si wafer. Prior to deposition, Si (100) wafers were cleaned ultrasonically in soap solution, acetone, and ethyl alcohol.

2.2. Pulsed laser deposition (PLD) apparatus and methodology

The cleaned substrates were mounted on a substrate holder inside the deposition chamber and placed parallel to the target at a perpendicular distance of 45 mm. The targets were continuously rotated to ensure uniform ablation and avoid pitting. KrF excimer laser system (Lambda Physik COMPEX) was used to deposit the YSZ, Al_2O_3, and Al_2O_3/YSZ multilayer films. The laser source with a wavelength of 248 nm, beam diameter of ~ 4 mm and pulsed duration of ~25 ns was operated at a pulse repetition rate of 10 Hz and at an energy density of ~ 2 J/cm^2. The total time for deposition was 50 minutes (30000 pulses). Films were deposited at substrate temperatures of 300 K, 573 K, 773 K, and 973 K. Prior to the initiation of deposition, the

deposition chamber was initially evacuated to 2.0×10^{-5} mbar and subsequently, filled with oxygen gas to a background pressure of 2×10^{-2} mbar.

2.3. Techniques for characterization of the pulsed laser deposited thin films

Following PLD, a detailed observation of the microstructure of the as-deposited films was undertaken by field emission scanning electron microscopy (FESEM, SUPRA 40, Zeiss SMT AG,Germany) and transmission electron microscopy (JEM 2100, JEOL Ltd, Tokyo, Japan). Specimens were prepared for planar and cross-sectional view under transmission electron microscope (TEM) by mechanically thinning and using a dimpler (Model 656, Gatan Inc., Pleasanton, CA, USA), followed by argon ion milling on a precision ion polishing system (Model 691, Gatan Inc., Pleasanton, CA, USA). An accelerating voltage of 200 kV was chosen during TEM operation. The phases present were identified by selected area electron diffraction (SAED) pattern analysis. The thickness of the pulsed laser deposited thin films was measured by surface profilometer (Dektak 150 surface profiler, Veeco Instruments, USA). Masking was done on the surface of substrate before deposition to ensure formation of a step between the deposited film and the substrate. A diamond tip stylus with radius 12.5 μm operating in contact mode under a normal load of 30 μN was allowed to scan through the step generated due to masking. An average measurement of five readings of the height of the step was considered to be the film thickness. A detailed analysis of the phase evolution was carried out by grazing incidence X-ray diffraction (GIXRD) technique (Bruker D8 Discover, Germany) with a grazing angle of 2° at a scanning speed of 0.05°/s using Cu Kα radiation. The crystallite size and lattice strain were performed using Scherrer's equation [30]. Residual stress developed on the surface of the thin films was carefully measured by XRD technique ($\sin^2\Psi$ method) using a Bragg Brentano Diffractometer (Bruker D8 Discover, Germany). For the calculation of residual stress, the (103)

peak of tetragonal zirconia phase was considered. The surface morphology and roughness of the deposited thin films were analyzed by atomic force microscopy (Agilent 5500 AFM, USA).

3. RESULTS AND DISCUSSION

3.1. Phase analysis using GIXRD

Figure 4 shows the XRD profiles of YSZ thin films deposited on Si (100) substrate at different substrate temperatures (T_s). From Figure 4, it can be seen that the thin film deposited at T_s = 300 K shows the signature of amorphous feature, while the films deposited at higher temperatures (573 K to 973 K) show polycrystalline tetragonal zirconia (t -ZrO_2). The amorphous nature of the thin film deposited at T_s = 300 K is due to poor adatom mobility on the surface of the substrate and hence, poor kinetics of diffusion as the ad-atoms cannot arrive at the vacant lattice site to take its position. On the other hand, with increase in substrate temperature, adatoms get the necessary energy for surface diffusion and fill up the vacant lattice site in an effort to make the film crystalline. A close comparison between Figure 1 and Figure 4 suggests that the deposited thin films are composed of 100% t-ZrO_2 phase with no signature of m-ZrO_2 phase. The complete transformation of m-ZrO_2 phase to t-ZrO_2 phase is attributed to the lowering of m-ZrO_2 to t-ZrO_2 transformation temperature under the non-equilibrium conditions of laser induced ablation during pulsed laser deposition [31]. Hence, it can be concluded that pulsed laser deposition is an effective deposition method for the development of stabilized tetragonal zirconia films. Table 1 summarizes the crystallite size and lattice strain induced in the thin films. The average crystallite size in YSZ thin film deposited at T_s = 573 K and 773 K was found to be constant (13 nm) as shown in Table 1. However, a marginal increase in crystallite size (15 nm) in the YSZ film deposited at T_s = 973 K is observed. From Table 1, it may be noted that the lattice strain in YSZ films varies from 0.69% to 0.77%. The marginal decrease in lattice strain at higher substrate

temperature may be attributed to stress relaxation due to higher mobility of adatoms due to increase in supply of thermal energy at higher substrate temperature.

Figure 5 shows the XRD profiles of Al_2O_3 thin films deposited on Si (100) substrate at 300 K (plot 1), 573 K (plot 2), 773 K (plot 3), and 973 K (plot 4). From plot 1, it can be seen that the deposited Al_2O_3 film is found to be amorphous which is attributed to the poor adatom mobility due to very low substrate temperature. However, with increase in substrate temperature there is no signature of crystallization of Al_2O_3 film. This observation indicates that a high temperature deposition up to 973 K is not sufficient to provide the required thermal energy for adatom mobility and as a result of which the grown films are found to be amorphous.

3.2. Microstructural characterization

Figure 6 shows FESEM micrographs of cross-section of YSZ thin films deposited on Si (100) substrate at (a) 300 K, (b) 573 K, (c) 773 K, and (d) 973 K. From Figure 6, it can be noted that the deposited thin films are grown in columnar fashion. There is presence of thick inter-columnar boundaries when deposition is carried out at room temperature which is not found in YSZ films deposited at higher T_s i.e. 573 K, 773 K, and 973 K. The thin film obtained at T_s = 973 K is found to be most dense. The decrease in intercolumnar gaps/porosity is attributed to the increase in thermal energy of the adatoms resulting denser thin film as a result of increase in T_s.

Figure 7 shows the FESEM micrographs of the top surface of YSZ films deposited at (a, b) 300 K, (c, d) 573 K, (e, f) 773 K, and (g, h) 973 K. Where (b), (d), and (e) shows the high magnification view of (a), (c), (e), and (g), respectively. From Figure 7a and Figure 7b, it may be noted that there are presence of a large number of particles on the surface of deposited YSZ films at 300 K with size ranging from 100 nm to 550 nm. From Figure 7c and Figure 7d, it may be noted that the film deposited at 573 K shows particle formation on the surface with particle size

ranging from ~ 50 nm to 1.5 μm. However, films deposited at 773 K and 973 K shows improved surface features with very less particle formation. The formations of particles are commonly observed due to laser induced splashing of molten materials from the target and subsequent condensation in vapor phase leads to the formation of droplets on the surface of YSZ film deposited by PLD. The size of the droplets varies with laser fluence [32]. The reduced density of the particles on the film surface with increase in substrate temperature may be attributed to the unavailability of low temperature sites to condense the liquid droplets with increase in substrate temperature. From Figure 7a to Figure 7h, it may be noted that the shape of particles is found to change from spherical shape at low temperature regime to flake type or faceted at high temperature regime.

Figure 8 shows the FESEM micrographs of the cross-section of Al_2O_3 thin films deposited at (a) 300 K, (b) 573 K, (c) 773 K, and (d) 973 K. From Figure 8a to Figure 8d, it may be noted that the deposited films are grown in columnar fashion. The thickness of the films is found to vary with substrate temperature T_s. The thickness of the Al_2O_3 thin film deposited at T_s = 973 K is found to be highest (2.3 μm) as compared to the films deposited at T_s = 300 K, 573 K, and 773 K.

Figure 9 shows the FESEM micrographs of top surface of Al_2O_3 films deposited at (a, b) 300 K, (c, d) 573 K, (e, f) 773 K, and (g, h) 973 K. Where (b), (d), and (e) shows the high magnification view of (a), (c), (e), and (g), respectively. From Figure 9a to Figure 9h, it may be noted that the presence of particles or droplets is observed on the top surface microstructure whose density decreases with increase in substrate temperature. From Figure 9a and Figure 9b, it is observed that the Al_2O_3 film deposited at T_s = 300 K contains many porosities and fine microcracks. With increase in substrate temperature the deposited films of Al_2O_3 shows

improved surface microstructure by showing decreased porosities and microcracks. The dense nature of the Al_2O_3 films with increase in substrate temperature is evident from Figure 9c to Figure 9h.

It has been found that a multilayer TBC architecture decreases the thermal conductivity of the TBC system [33]. The presence of interfaces between the successive films was responsible for reduction in thermal conductivity due to thermal resistance offered by these interfaces. Hence, a multilayer thin film of Al_2O_3 and YSZ was fabricated. Figure 10 shows the FESEM micrographs of the (a) top surface of the Al_2O_3/YSZ multilayer thin film and (b) cross-section of the Al_2O_3/YSZ multilayer thin film. From Figure 10a, it may be noted that presence of large number of particles on the surface of Al_2O_3/YSZ multilayer thin film. The size of the particles was found to vary from few hundreds of nanometer to ~ 2.5 μm. The formation of particles on the surface of Al_2O_3/YSZ multilayer thin film may be attributed to "*splashing effect*" as explained in earlier section. From Figure10b, it may be noted that the cross-section of Al_2O_3/YSZ multilayer thin film showed almost uniform thickness of ~ 320 nm. The columnar growth of the film is observed from Figure 10b. However, intercolumanr gaps are evident from the microstructure of the Al_2O_3/YSZ multilayer thin film.

Figure 11 shows the (a) plan view bright field TEM image and (b) corresponding SAED pattern of pulsed laser deposited YSZ thin film grown at room temperature. From Figure 11a, it may be seen that the YSZ thin film is predominantly amorphous structure with few crystallites distributed in it when deposition was conducted at room temperature. The grain size is found to be ~ 70 nm. The formation of diffusion rings in the SAED pattern confirms amorphous matrix; however, some diffraction spots are also found which contradicts XRD results at room temperature. The difference arises due to the fact that XRD gives the average result over a large

area, whereas TEM shows atomic level result in localized area. However, it has also been reported that the crystallization of YSZ thin film occurs by energetic electron beam in TEM [34].

Figure 12 shows (a) plan view bright field TEM image, (b) corresponding SAED pattern, and (c) high resolution transmission electron microscopy image of pulsed laser deposited YSZ thin films at 973 K. From Figure 12a, it can be seen that the structure is polycrystalline in nature. The ring pattern as shown in Figure 12b is found as tetragonal zirconia structure which matches well with GIXRD result. The grain size was found to be ~ 55 nm. HRTEM image showing lattice fringe is also confirmed from the lattice fringe showing an interplanar spacing $d_{(101)}$ of 0.295 nm as shown in Figure 12c which matches well with tetragonal zirconia structure.

Figure 13 shows the (a) plan view bright field TEM image and (b) corresponding SAED pattern of Al_2O_3 thin films deposited at T_s = 300 K. From Figure 13, it may be noted that the film is amorphous in nature as no diffraction spot or ring patterns are found in SAED pattern. However, the contrast observed in the TEM image may be attributed to the mass thickness contrast due to presence of particulates. Presence of fine porosities/cracks and particles may be evident from the microstructure.

Figure 14 shows the (a) plan view bright field TEM image and (b) corresponding SAED pattern of Al_2O_3 thin films deposited at T_s = 973 K. With increase in substrate temperature, no crystallite was found in the microstructure and the SAED patter indicates amorphous nature of the film. The microstructure of the film deposited at 973 K shows uniform and dense film. Unlike Figure 14, no contrast is observed in the microstructure which indicates neither crystallites nor mass thickness variation which may be due to decrease in particulate formation. The TEM results obtained for Al_2O_3 thin films at 300 K and 973 K may be corroborated with the GIXRD results discussed elsewhere.

Figure 15 shows the cross-sectional TEM image of Al_2O_3/YSZ multilayer thin film deposited on Si (100) substrate at 300 K. The micrograph clearly shows formation of multilayered structure with Al_2O_3 as a first layer near to silicon substrate and YSZ as the top outer layer. The thickness of single layer of YSZ and Al_2O_3 was found to be ~ 100 nm and ~ 20 nm, respectively. Careful observation of Figure 15 indicated presence of few crystallites microstructure of YSZ.

3.3. Surface topography analysis

Figure 16 shows the surface topography of the pulsed laser deposited YSZ films at (a) 300 K, (b) 573 K, (c) 773 K, and (d) 973 K. From Figure 16a, it may be noted that nonuniform structure was formed at lower substrate temperature. The RMS roughness of YSZ film deposited at 300 K was found to be 12.9 nm. From Figure 16b to Figure 16d, it may be noted that the particle density is found to decrease with increase in substrate temperature. With increase in substrate temperature, the columnar growth of grain is observed. At a substrate temperature of 973 K, the film is found to be dense and columnar indicating the formation of crystalline film. The RMS roughness at 573 K, 773 K, and 973 K are found to be 9.66 nm, 4.79 nm, and 4.28 nm, respectively. The maximum heights of the features present in the YSZ film deposited at 300 K, 573 K, 773 K, and 973 K are found to be ~ 220 nm, 90 nm, 45 nm, and 27 nm, respectively. The RMS roughness is found to decrease with increase in substrate temperature which is attributed to the decrease in particle height on the surface of YSZ film with increase in substrate temperature, T_s.

Figure 17 shows the surface topography of the pulsed laser deposited Al_2O_3 films at (a) 300 K, (b) 573 K, (c) 773 K, and (d) 973 K. From Figure 17a, it may be noted that there are presence of particulates at lower substrate temperature. The maximum height of these features is

found to be 75 nm. The RMS roughness of Al_2O_3 film deposited at 300 K is found to be 7.31 nm. The RMS roughness at 573 K, 773 K, and 973 K are found to be 3.3 nm, 2 nm, and 0.91 nm, respectively. The RMS roughness is found to decrease with increase in substrate temperature which is attributed to the decrease in particle height on the surface of Al_2O_3 film with increase in substrate temperature, T_s. The maximum heights of the features present in the Al_2O_3 film deposited at 573 K, 773 K, and 973 K are found to be ~ 26 nm, 15 nm, and 13 nm, respectively. With increase in substrate temperature, the columnar grain growth is not observed in the deposited films which indicate absence of crystallinity in the deposited films. Figure 18 shows the AFM image of top surface of Al_2O_3/YSZ multilayer thin film. From Figure 18, it may be noted that spherical grains are observed on the surface of the film which is also evident from Figure 10.

3.4. Residual stress analysis

The residual stress developed in YSZ thin films was measured by XRD technique and are summarized in Table 2. From Table 2, it is evident that the residual stress in the deposited films decreases with increase in substrate temperature. The residual stresses are predominantly compressive in nature at all substrate temperature. At T_s = 573 K, the residual stress component σ_{11} is found to be -8.1 GPa which reduces to -3.0 GPa at T_s = 973 K. Similarly, the residual stress component σ_{22} is found to be -6.4 GPa and at T_s = 573 K, which decreases to -1.7 GPa at 773 K. The higher residual compressive stress at low substrate temperature is attributed to the impingement of highly energetic species present in the plume on to the substrate or on to the growing films. The reduction in residual stress with increase in substrate temperature is attributed to the better surface diffusion of adatoms and release of stress with increase in temperature [35, 36].

4. SUMMARY & CONCLUSIONS

In the present study, the microstructural characterization of pulsed laser deposited yttria stabilized zirconia (YSZ) and alumina (Al_2O_3) thin films are studied in detail. From the detailed investigations, the following conclusions may be drawn:

1. XRD phase analysis of YSZ powder and pallets (used for target preparation) show the formation of monoclinic as well as tetragonal zirconia. The volume fraction of monoclinic zirconia phase in YSZ pallet decreased from 29.1 % to 2.6 % and the volume fraction of tetragonal zirconia phase in sintered pallet increases from 70.9 % to 97.4%. Presence of only α - Al_2O_3 phase was observed in both powder and sintered pellet.

2. XRD phase analysis of YSZ films deposited at room temperature showed amorphous feature, while the film deposited at high temperature showed crystalline behavior. The phase analysis at higher substrate temperature showed formation of tetragonal phase only with no signature of monoclinic zirconia. Crystallite size and lattice strain was not found to vary with increase in substrate temperature. However, the TEM analysis indicated the amorphous nature of the matrix with few crystallites distributed in it. On the other hand, no crystalline peaks in the XRD of Al_2O_3 thin films were observed at room temperature as well as at high temperature which were verified with TEM results.

3. Residual stress analysis of the coating at all temperature showed the presence of compressive stress and was maximum at Ts = 573 K ($\sigma11$ = -8.1 GPa and $\sigma22$ = -6.4 GPa) and minimum at Ts = 973 K ($\sigma11$ = -3.0 GPa and $\sigma22$ = -1.7 GPa).

4. The cross-sectional morphology of YSZ and Al_2O_3 thin films deposited at room temperature showed presence of intercolumnar porosities which changed to a dense structure

with increase in substrate temperature. The top surface microstructure of YSZ films deposited at room temperature showed presence of large number of particles. With increase in substrate temperature the particles density was decreased and the surface was found to be smooth.

5. The morphology of YSZ film as evident from AFM image showed higher RMS roughness (12.9 nm) at room temperature which decreases with increase in substrate temperature. The room temperature morphology is nonuniform, whereas with increase in substrate temperature, the directional growth of grain was observed in YSZ films. The RMS roughness for both the films decreases with increase in temperature.

ACKNOWLEDGEMENTS

The partial financial support for this work from the Alexander von Humboldt Foundation, Department of Science and Technology (DST), New Delhi and the Council of Scientific and Industrial Research, New Delhi are gratefully acknowledged.

REFERENCES

[1] Miller, R.A. (1997). Thermal barrier coatings for aircraft engines: history and directions. *Journal of Thermal Spray Technology*, 6 (1), 35–42.

[2] Li, J.F., Liao, H., Wang, X.Y., Normand, B., Ji, V., Ding, C.X., Coddet, C. (2004). Improvement in wear resistance of plasma sprayed yttria stabilized zirconia coating using nanostructured powder. *Tribology International*, 37 (1), 77–84.

[3] Evans, A. G., Mumm, D. R., Hutchinson, J. W., Meier, G. H., Pettit F. S. (2001). Mechanisms controlling the durability of thermal barrier coatings. *Progress in Materials Science*, 46 (5), 505–553.

[4] Haile, S. M. (2003). Fuel cell materials and components. *Acta Materialia*, 51 (19), 5981–6000.

[5] Brandont, R., Taylor, R. (1991). Phase stability of zirconia-based thermal barrier coatings part I. Zirconia—yttria alloys. *Surface and Coating Technology*, 46 (1), 75–90.

[6] Nie, X., Meletis, E. I., Jiang, J. C., Leyland, A., Yerokhin, A. L., Matthews, A. (2002). Abrasive wear corrosion properties and TEM analysis of Al_2O_3 coatings fabricated using plasma electrolysis. *Surface and Coating Technology*, 149 (2–3), 245–251.

[7] Aryasomayajula, A., Canovic, S., Bhat, D., Gordon, M. H., Halvarsson, M. (2007). Transmission electron microscopy and X-ray diffraction analysis of alumina coating by alternate-current inverted magnetron-sputtering technique. *Thin Solid Films*, 516 (2–4), 397–401.

[8] Shin, J., Goyal, A., Wee, S. (2009). Growth of epitaxial γ-Al_2O_3 films on rigid single-crystal ceramic substrates and flexible, single-crystal-like metallic substrates by pulsed laser deposition. *Thin Solid Films*, 517 (19), 5710–5714.

[9] Sun, J. H., Chang, E., Chao C. H., Cheng, M. J. (1993). The spalling modes and degradation mechanism of ZrO_2-8 wt.% Y_2O_3/CVD-Al_2O_3/Ni-22Cr-10Al-1Y thermal-barrier coatings. *Oxidation of Metals*, 40 (5–6), 465–481.

[10] Widjaja, S., Limarga A. M., Yip, T. H. (2002). Oxidation behavior of a plasma-sprayed functionally graded ZrO_2/Al_2O_3 thermal barrier coating. *Material Letters*, 57 (3), 628–634.

[11] Su, Y. F., Allard, L.F., Coffey, D.W., Lee, W.Y. (2004). Effects of an α-Al_2O_3 Thin film on the oxidation behavior of a single-crystal Ni-based superalloy, *Metallurgical and Materials Transactions A*, 35 (3), 1055–1065.

[12] Balakrishnan, G., Kuppusami, P., Tripura Sundari, S., Thirumurugesan, R., Ganesan, V., Mohandas, E., Sastikumar, D. (2010). Structural and optical properties of γ-alumina thin films prepared by pulsed laser deposition, *Thin Solid Films*, 518 (14), 3898–3902.

[13] Zhang, X., Ren, W., Shi, P., Tian A., Xin, H., Chen, X., Wu, X., Yao, X. (2010). Influence of substrate temperature on structures and dielectric properties of pyrochlore $Bi_{1.5}Zn_{1.0}Nb_{1.5}O_7$ thin films prepared by pulsed laser deposition. *Applied Surface Science*, 256 (22), 6607–6611.

[14] Cho, C. R., Grishin, A. (1999). Self-assembling ferroelectric $Na_{0.5}K_{0.5}NbO_3$ thin films by pulsed-laser deposition. *Applied Physics Letter*, 75 (2), 268–270.

[15] Pillonnet, A., Garapon, C., Champeaux, C., Bovier, C., Brenier, R., Jaffrezic, H., Mugnier J. (1999). Influence of oxygen pressure on structural and optical properties of Al_2O_3 optical waveguides prepared by pulsed laser deposition, *Applied Physics A*, 69 (1), S735–S738.

[16] Balakrishnan, G., Tripura Sundari, S., Ramaseshan, R., Thirumurugesan, R., Mohandas, E., Sastikumar, D., Kuppusami, P., Kim, T. G., Song, J. I. (2013). Effect of substrate temperature on microstructure and optical properties of nanocrystalline alumina thin films. *Ceramic International*, 39 (8), 9017–902.

[18] Gsell, S., Fischer, M., Bauer, T., Schreck, M., Stritzker, B. (2006). Yttria-stabilized zirconia films of different composition as buffer layers for the deposition of epitaxial diamond/Ir layers on Si(001). *Diamond and Related Materials*, 15 (4–8), 479 – 485.

[19] Pryds, N., Toftmann, B., Bilde-Sørensen, J. B., Schou, J., Linderoth, S. (2006). Thickness determination of large-area films of yttria-stabilized zirconia produced by pulsed laser deposition. *Applied Surface Science*, 252 (13), 4882–4885.

[20] Caricato, A.P., Barucca, G., Di Cristoforo, A., Leggieri, G., Luches, A., Majni, G., Martino, M., Mengucci, P. (2005). Excimer pulsed laser deposition and annealing of YSZ nanometric films on Si substrates. *Applied Surface Science*, 248 (1–4), 270–275.

[21] Joo, J. H., Choi, G. M. (2006). Electrical conductivity of YSZ film grown by pulsed laser deposition. Solid State Ionics, 177 (11–12), 1053–1057.

[22] Rodrigo, K., Knudsen, J., Pryds, N., Schou, J., Linderoth, S. (2007). Characterization of yttria-stabilized zirconia thin films grown by pulsed laser deposition (PLD) on various substrates. *Applied Surface Science*, 254 (4), 1338–1342.

[23] Heiroth, S., Lippert, T., Wokaun, A., Döbeli, M., Rupp, J. L. M., Scherrer, B., Gauckler, L. J. (2010). Yttria-stabilized zirconia thin films by pulsed laser deposition: Microstructural and compositional control. *Journal of European Ceramic Society*, 30 (2), 489–495.

[24] Heiroth, S., Frison, R., Rupp, J. L. M., Lippert, T., Meier, E. J. B., Gubler, E. M., Döbeli, M., Conder, K., Wokaun, A., Gauckler, L. J., (2011). Crystallization and grain growth characteristics of yttria-stabilized zirconia thin films grown by pulsed laser deposition. *Solid State Ionics*, 191 (1), 12–23.

[25] Balakrishnan, G., Venkatesh Babu, R., Shin, K. S., Song, J. I. (2014). Growth of highly oriented γ- and α-Al_2O_3 thin films by pulsed laser deposition. *Optics & Laser Technology*, 56, 317–321.

[26] Singh, A. K., Kaity, S., Singh, K., Thomas, J., Kutty, T. R. G., Sinha, S. (2014). Pulsed laser deposition of alumina coating for corrosion protection against liquid uranium. *Materials Chemistry and Physics*, 143 (3), 1446 -1451

[27] Balakrishnan, G., Sairam, T.N., Kuppusami, P., Thiumurugesan, R., Mohandas, E., Ganesan, V., Sastikumar, D. (2011). Influence of oxygen partial pressure on the properties of pulsed laser deposited nanocrystalline zirconia thin films. *Applied Surface Science*, 257 (20), 8506–8510

[28] Balakrishnan, G., Kuppusami, P., Murugesan, S., Ghosh, C., Divakar, R., Mohandas, E., Ganesan, V., Sastikumar, D. (2012). Characterization of Al_2O_3/ZrO_2 nano multilayer thin films prepared by pulsed laser deposition. *Materials Chemistry and Physics*, 133 (1), 299–303.

[29] Miller, R. A., Smialek, J. L., Garlick, R. G. (1981). Phase stability in plasma-sprayed, partially stabilized zirconia–yttria. In *Conference Proceedings*: *Science and Technology of Zirconia*, pp. 241 – 253, Columbus, OH.

[30] Cullity, B.D. (1956). *Elements of X-ray diffraction* (2nd ed.). CA: Addison-Wesley.

[31] Mishra, M., Kuppusami, P., Singh, A., Ramya, S., Sivasubramanian, V., Mohandas, E. (2012). Phase evolution in zirconia thin films prepared by pulsed laser deposition, *Applied Surface Science*, 258 (12), 5157– 5165.

[32] Siew, W. O., Lee, W. K., Wong, H. Y., Yong, T. K., Yap, S. S., Tou, T. Y. (2010). Investigation of droplet formation in pulsed Nd:YAG laser deposition of metals and silicon. *Applied Physics A*, 101 (4), 627–632.

[33] Ravichandran, K. S., An, K., Dutton, R. E., Semiatin, S. L. (1999). Thermal conductivity of plasma-sprayed monolithic and multilayer coatings of alumina and yttria-stabilized zirconia. *Journal of American Ceramic Society*, 82 (3), 673–682.

[34] Heiroth, S., Frison, R., Rupp, J. L.M., Lippert, T., Meier, E. J. B., Gubler, E. M., Döbeli, M., Conder, K., Wokaun, A., Gauckler, L. J. (2011). Crystallization and grain growth characteristics of yttria-stabilized zirconia thin films grown by pulsed laser deposition. *Solid State Ionics*, 191 (1), 12–23.

[35] Tabbal, M., Kahwaji, S., Christidis, T.C., Nsouli, B., Zahraman, K. (2006). Pulsed laser deposition of nanostructured dichromium trioxide thin films. *Thin Solid Films*, 515 (4), 1976–1984.

[36] Xiong, J., Qin, W., Cui, X., Tao, B., Tang, J., Li, Y. (2006). Effect of processing conditions and methods on residual stress in CeO_2 buffer layers and YBCO superconducting films. *Physica C*, 442 (2), 124–128.

List of Figures

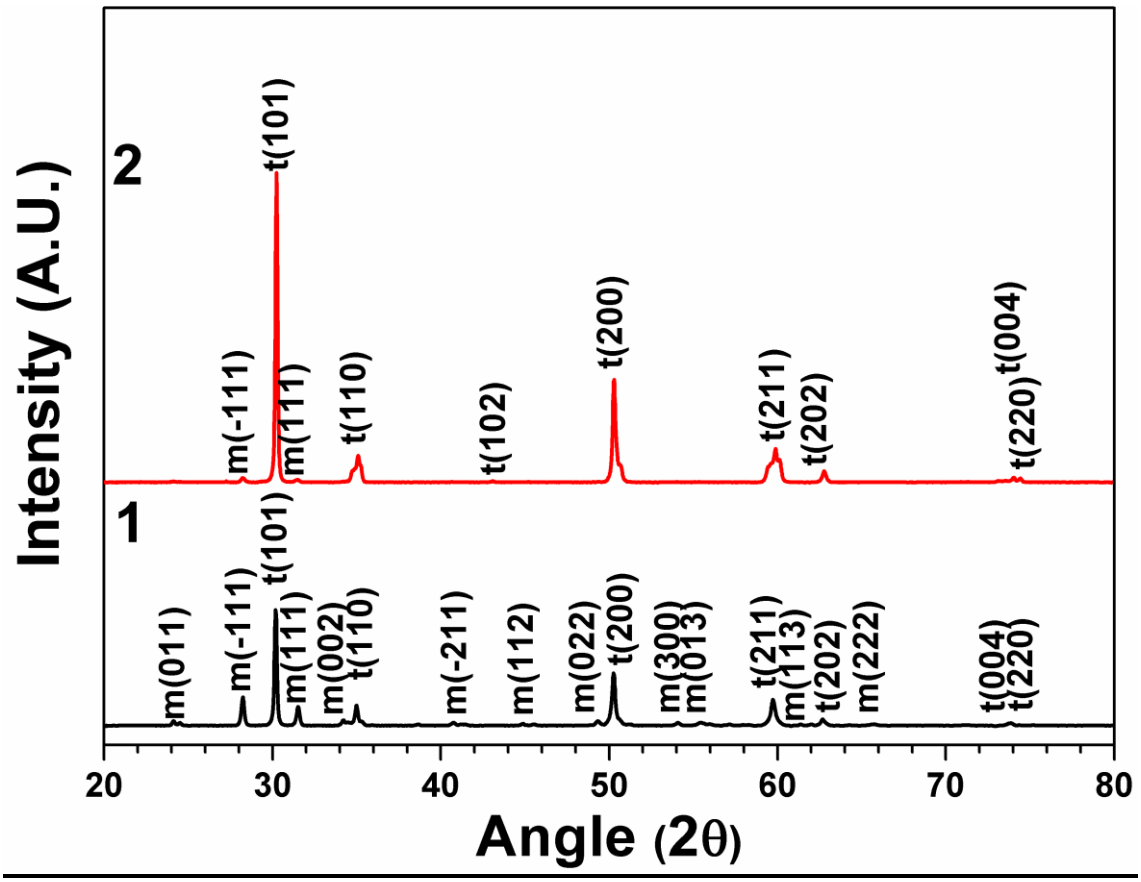

Figure 1 XRD profiles of YSZ powder (plot 1) and YSZ sintered pellet (plot 2).

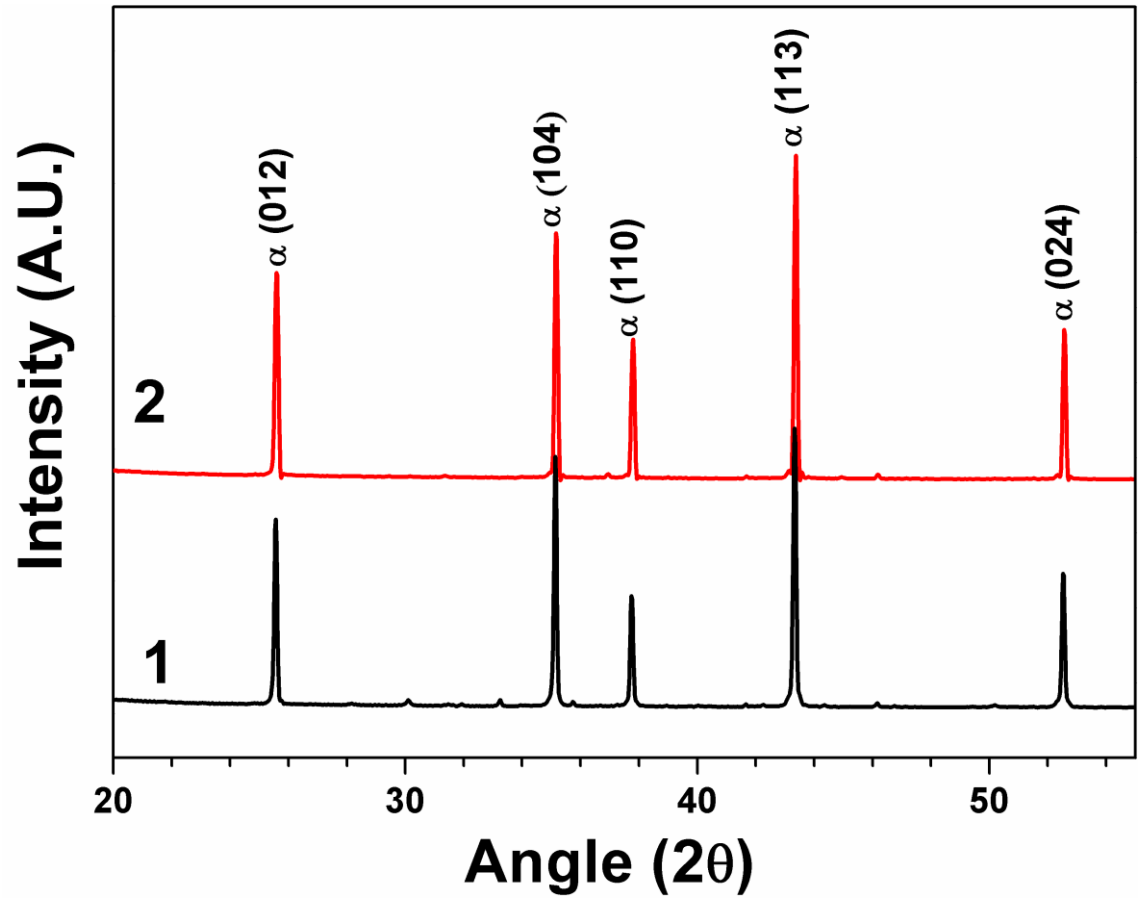

Figure 2 XRD profiles of Al_2O_3 powder (plot 1) and Al_2O_3 sintered pellet (plot 2).

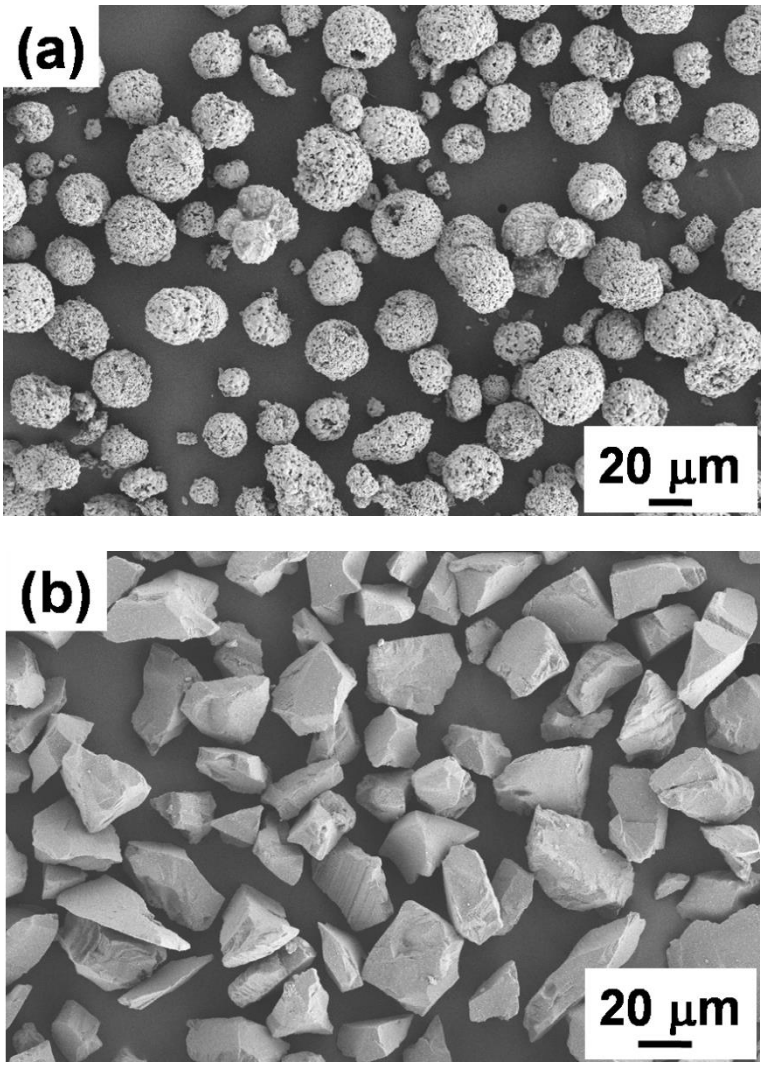

Figure 3 FESEM micrographs of (a) YSZ and (b) Al_2O_3 precursor powders.

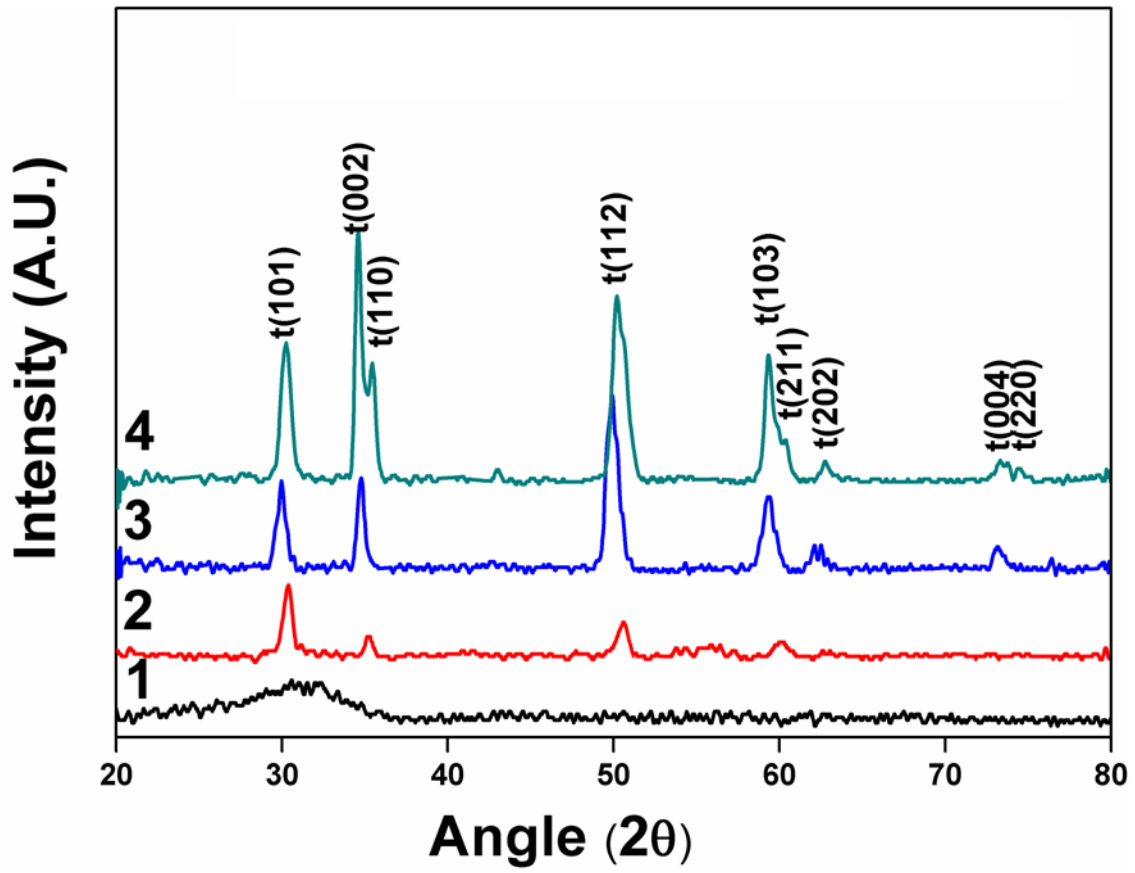

Figure 4 XRD profiles of YSZ thin film deposited on Si (100) at different substrate temperature of 300 K (plot 1), 573 K (plot 2), 773 K (plot 3), and 973 K (plot 4).

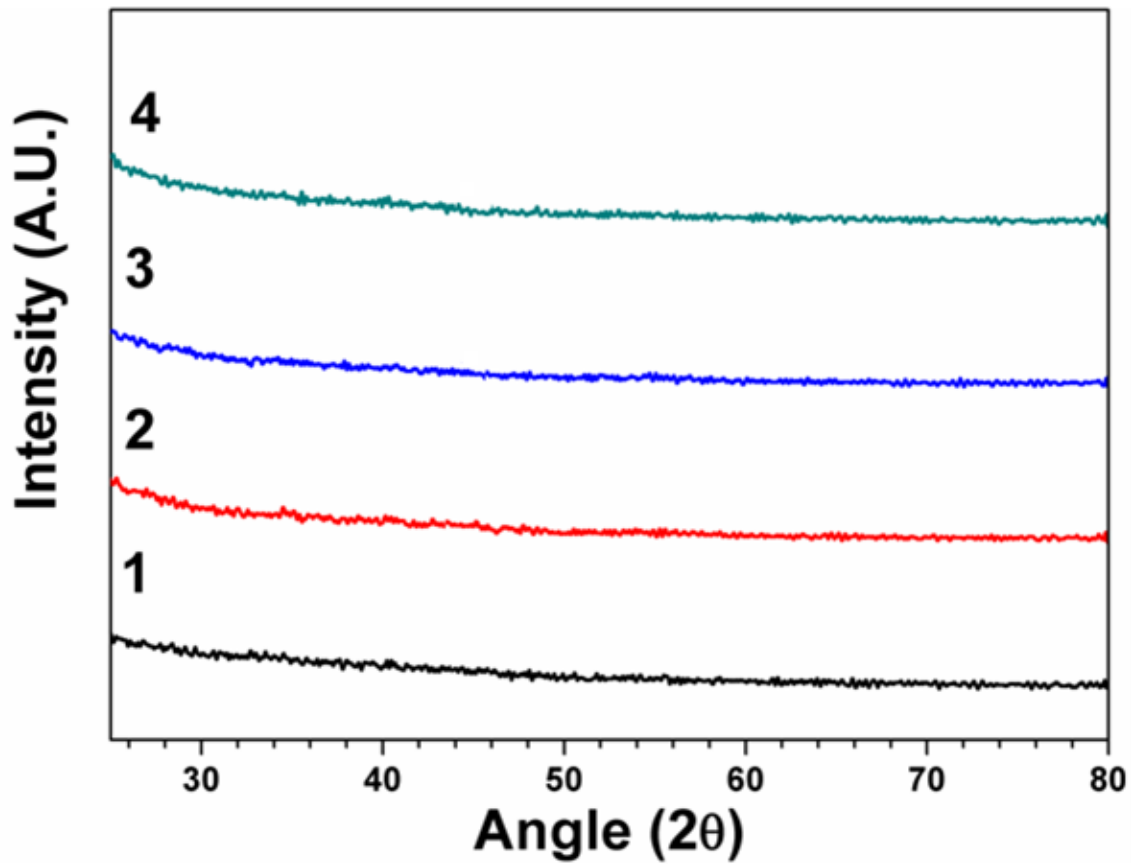

Figure 5 XRD profiles of Al_2O_3 thin film deposited on Si (100) substrate at 300 K (plot 1), 573 K (plot 2), 773 K (plot 3), and 973 K (plot 4).

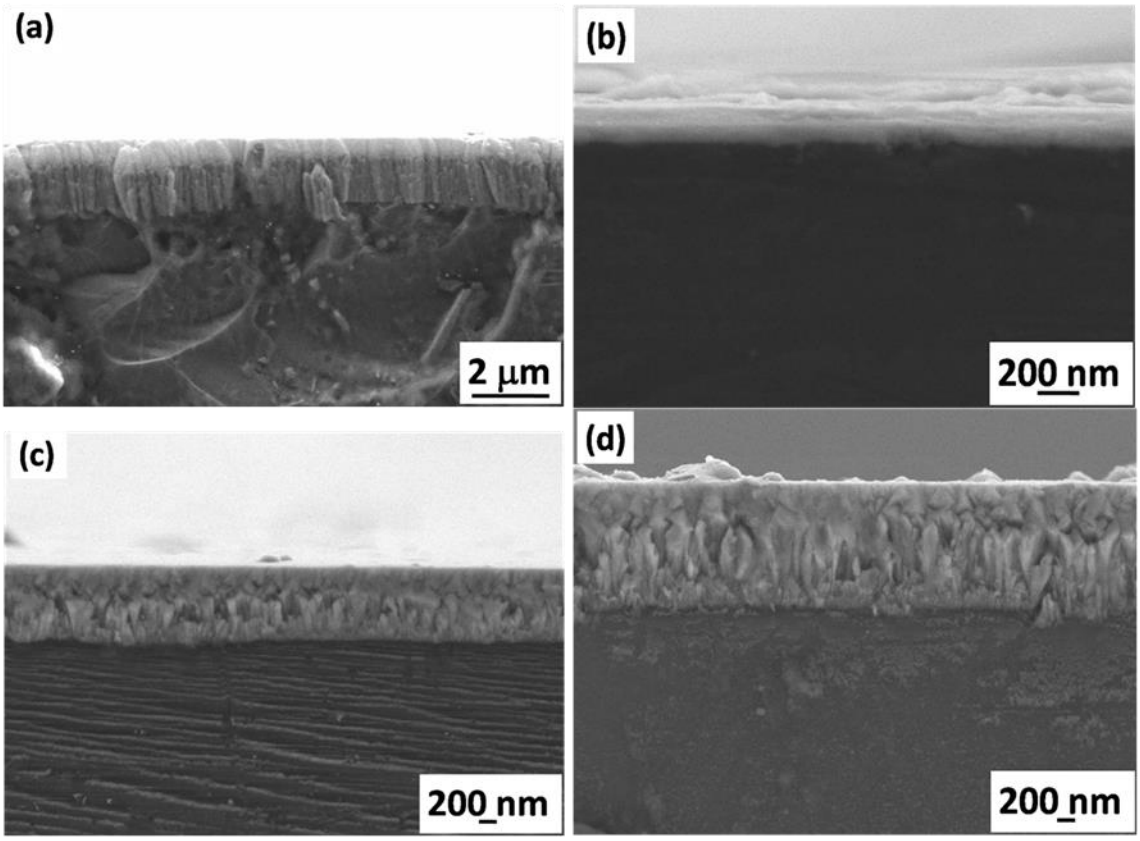

Figure 6 FESEM micrographs of cross-section of as-deposited YSZ thin films on Si (100) substrate at (a) 300 K, (b) 573 K, (c) 773 K, and (d) 973 K.

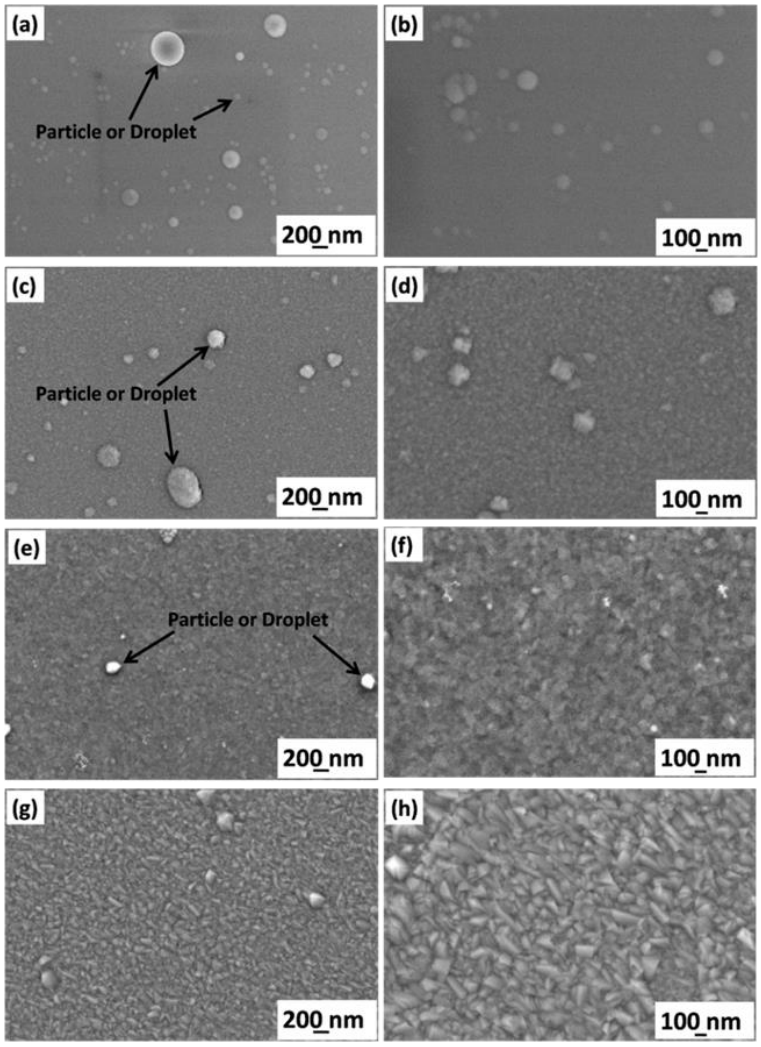

Figure 7 FESEM micrograph of top surface of as-deposited YSZ thin film at (a, b) 300 K, (c, d) 573 K, (e, f) 773 K, and (g, h) 973 K. Where (b), (d), and (e) shows the high magnification view of (a), (c), (e), and (g), respectively.

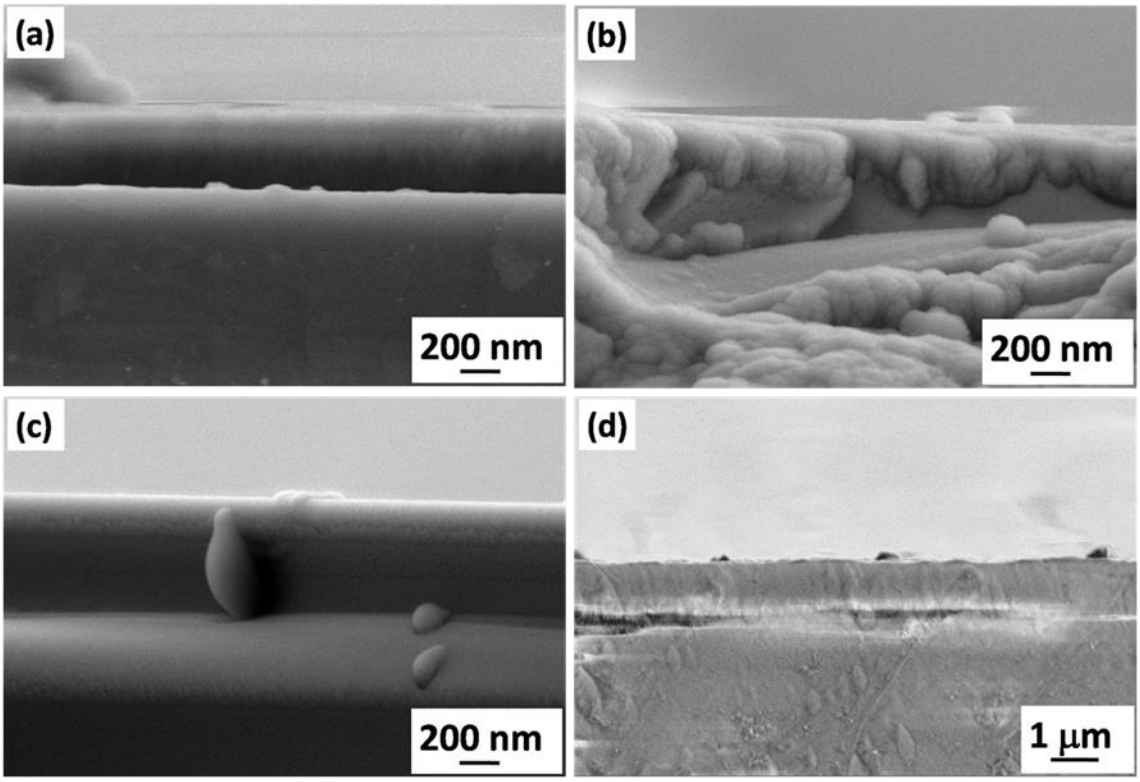

Figure 8 FESEM micrograph of cross-section surface of as-deposited Al_2O_3 thin film at (a) 300 K, (b) 573 K, (c) 773 K, and (d) 973 K.

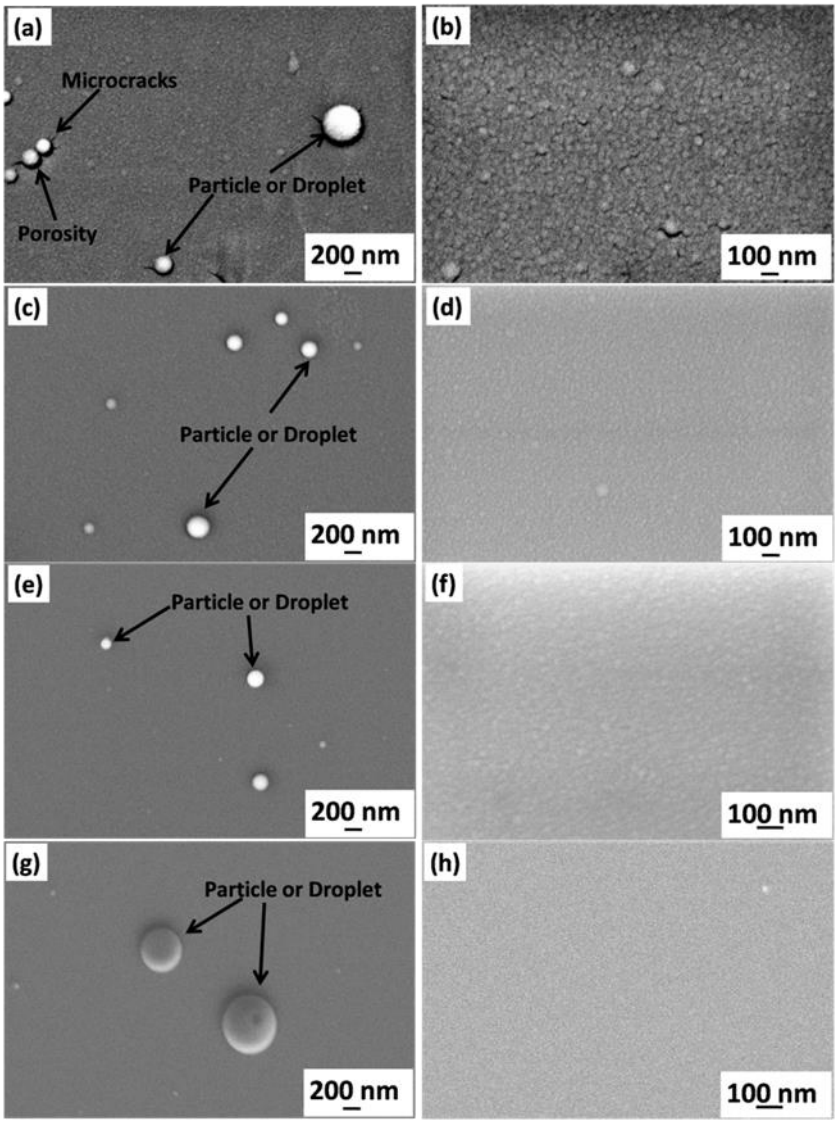

Figure 9 FESEM micrographs of top surface of as-deposited Al_2O_3 thin films at (a, b) 300 K, (c, d) 573 K, (e, f) 773 K, and (g, h) 973 K. Where (b), (d), and (e) shows the high magnification view of (a), (c), (e), and (g), respectively.

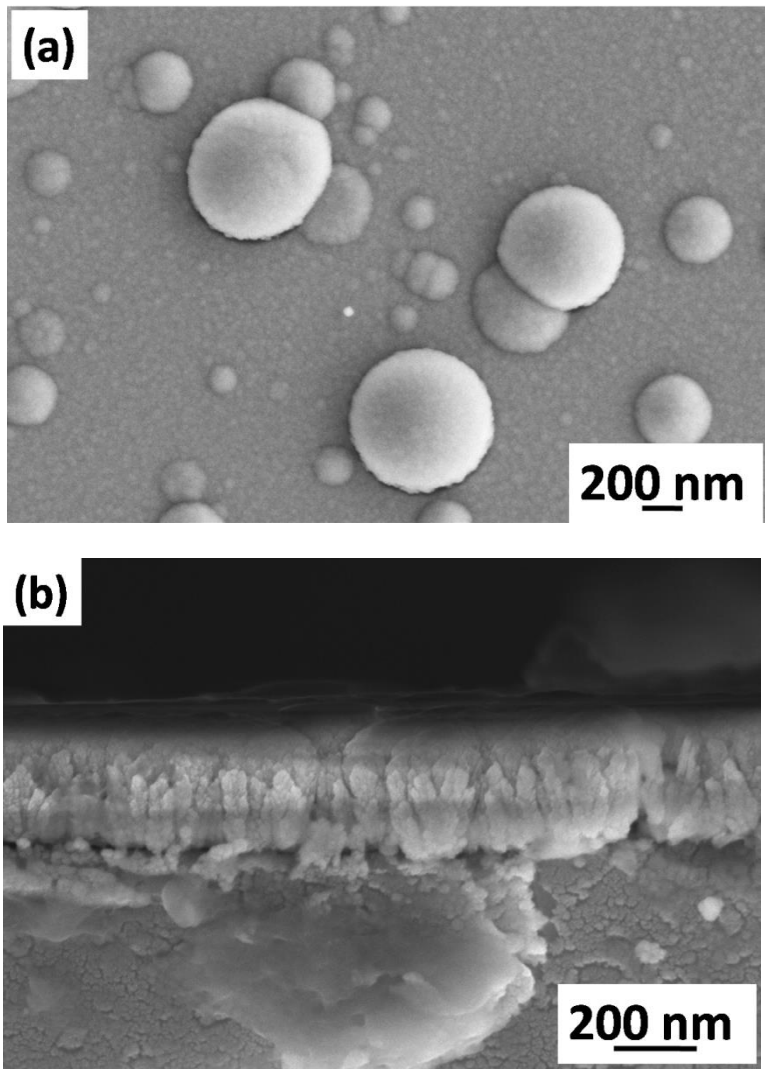

Figure 10 FESEM micrograph of as-deposited Al_2O_3/YSZ thin film showing microstructure of (a) top surface and (b) cross-section deposited on Si (100) substrate at 300 K.

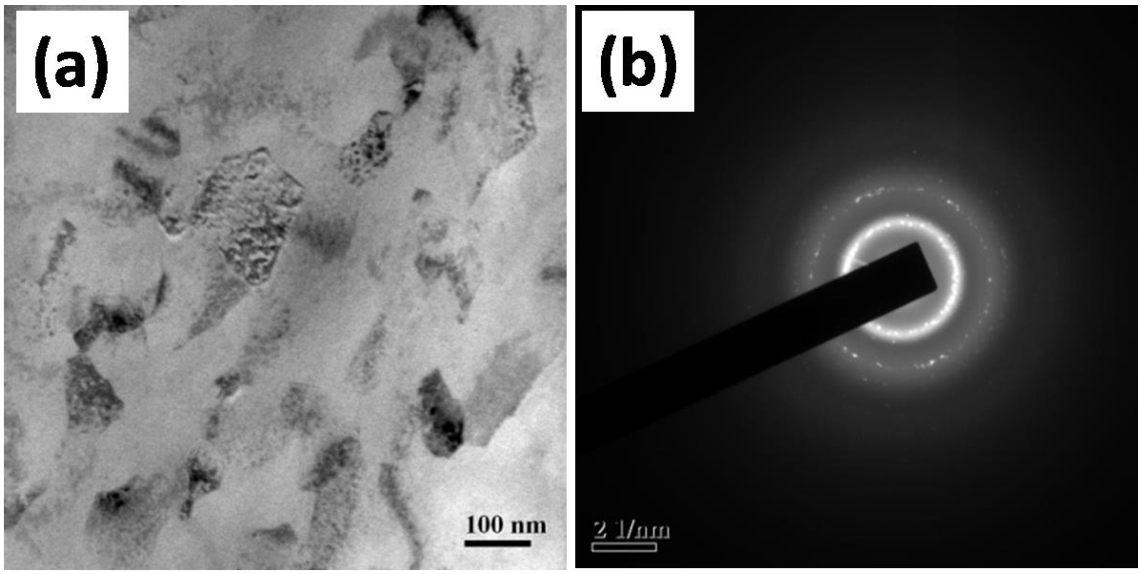

Figure 11 (a) Bright field transmission electron microscopy image and (b) corresponding SAD pattern of pulsed laser deposited YSZ thin films at 300 K.

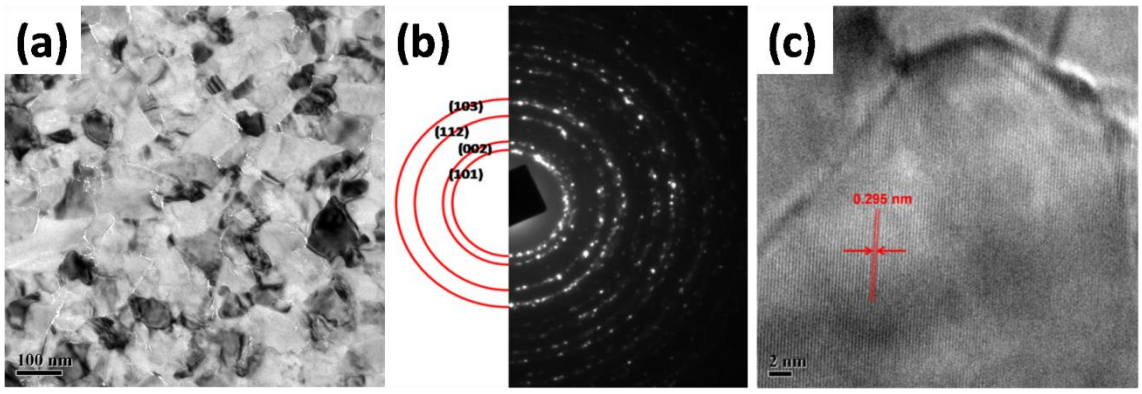

Figure 12 (a) Bright field transmission electron micrograph, (b) corresponding SAED pattern, and (c) high resolution transmission electron micrograph of pulsed laser deposited YSZ thin films at 973 K.

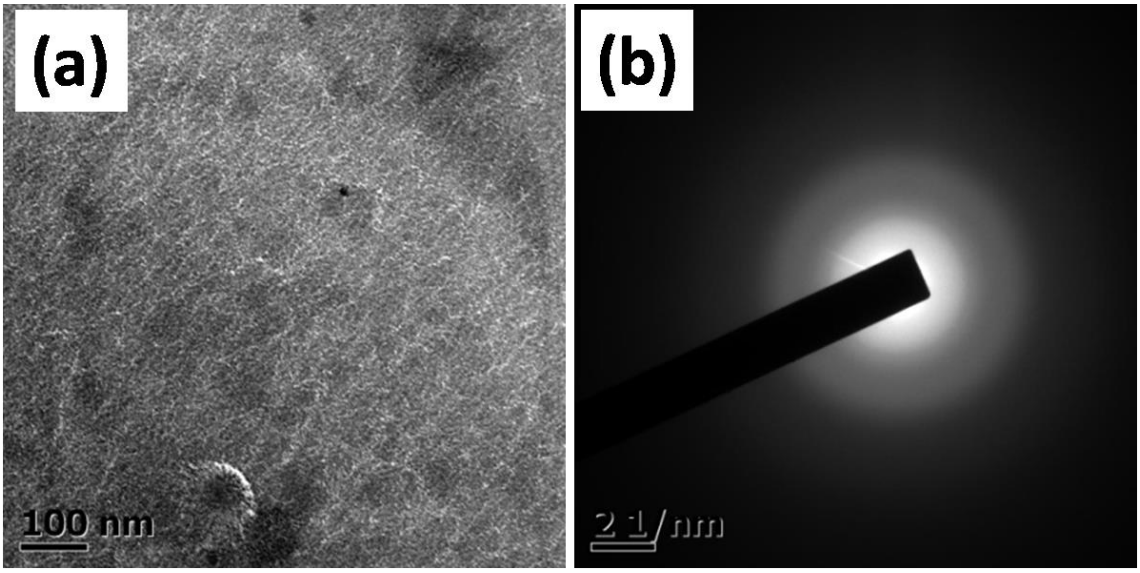

Figure 13 (a) Bright field transmission electron microscopy image of plan view and (b) corresponding SAED pattern of pulsed laser deposited Al_2O_3 thin films at 300 K.

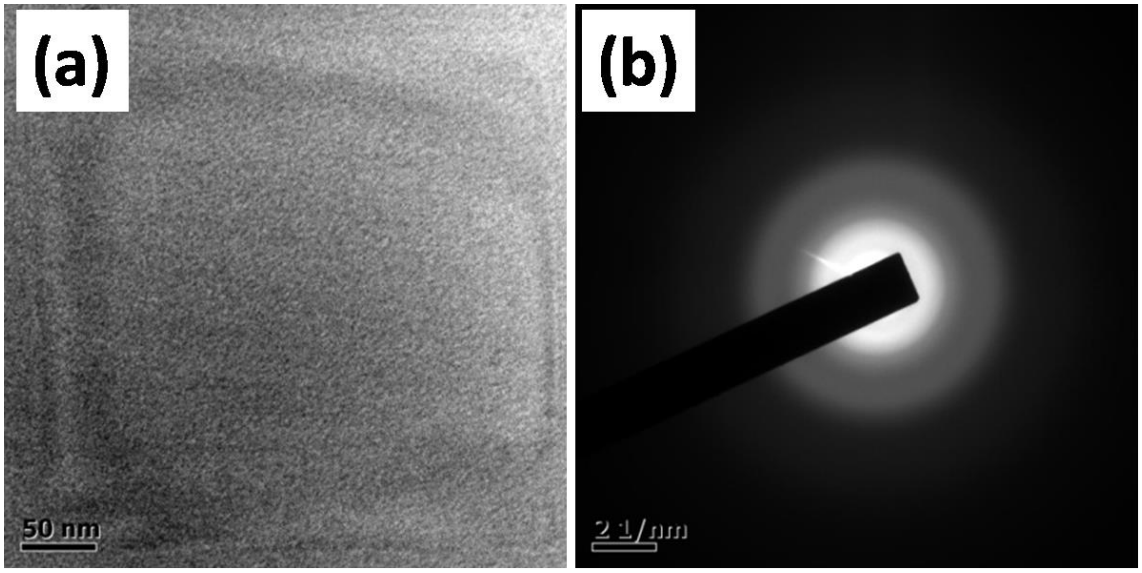

Figure 14 (a) Bright field transmission electron micrograph of plan view and (b) corresponding SAED pattern of pulsed laser deposited Al_2O_3 thin films at 973 K.

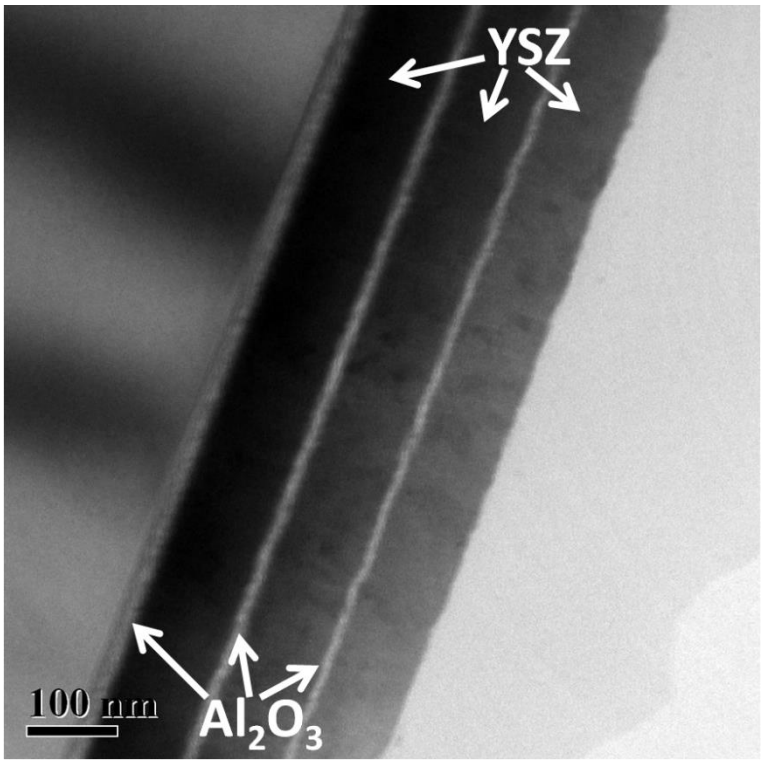

Figure 15 Bright field transmission electron micrograph of cross-section of Al_2O_3/YSZ multilayer thin film deposited at 300 K.

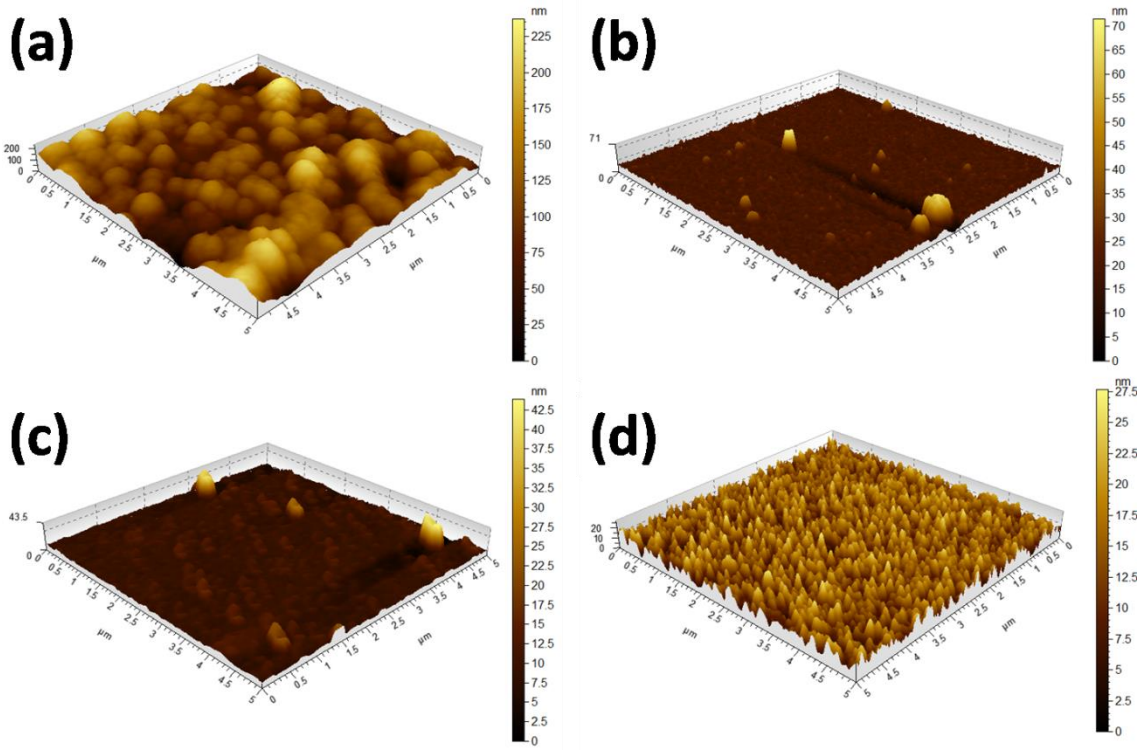

Figure 16 Atomic force microscope image of YSZ thin films grown at (a) 300 K, (b) 573 K, (c) 773 K, and (d) 973 K.

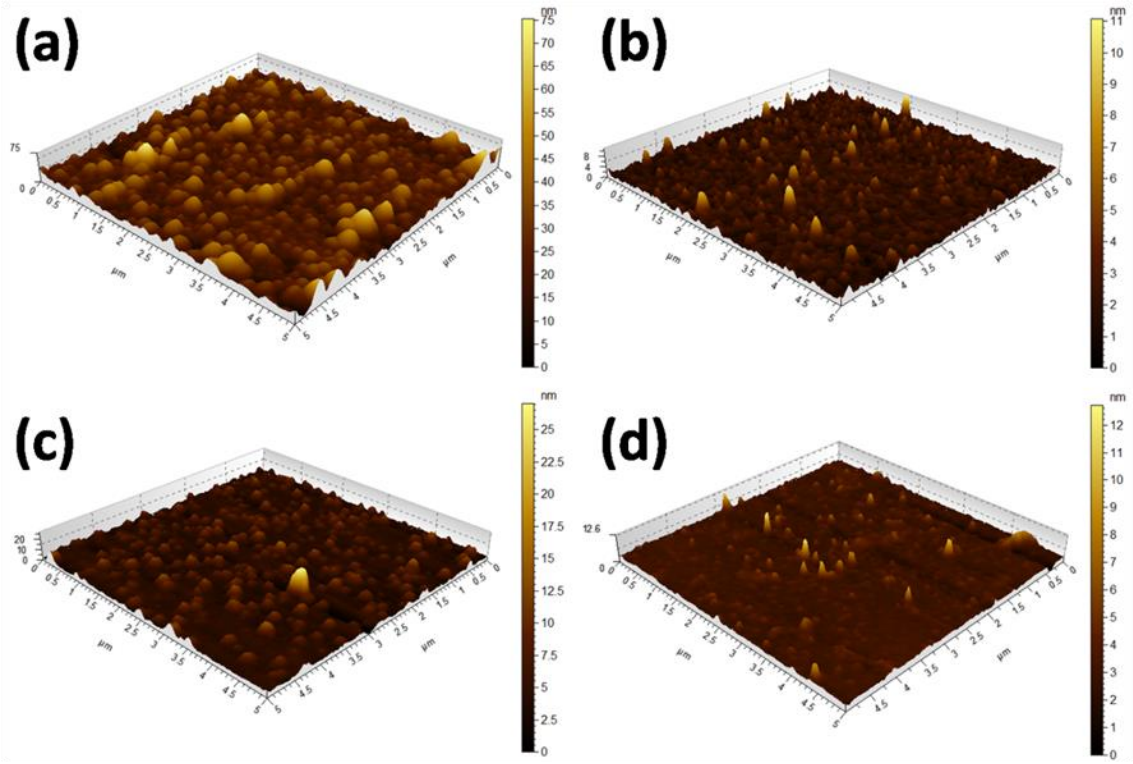

Figure 17 Atomic force microscope images of Al_2O_3 thin films grown at (a) 300 K, (b) 573 K, (c) 773 K, and (d) 973 K.

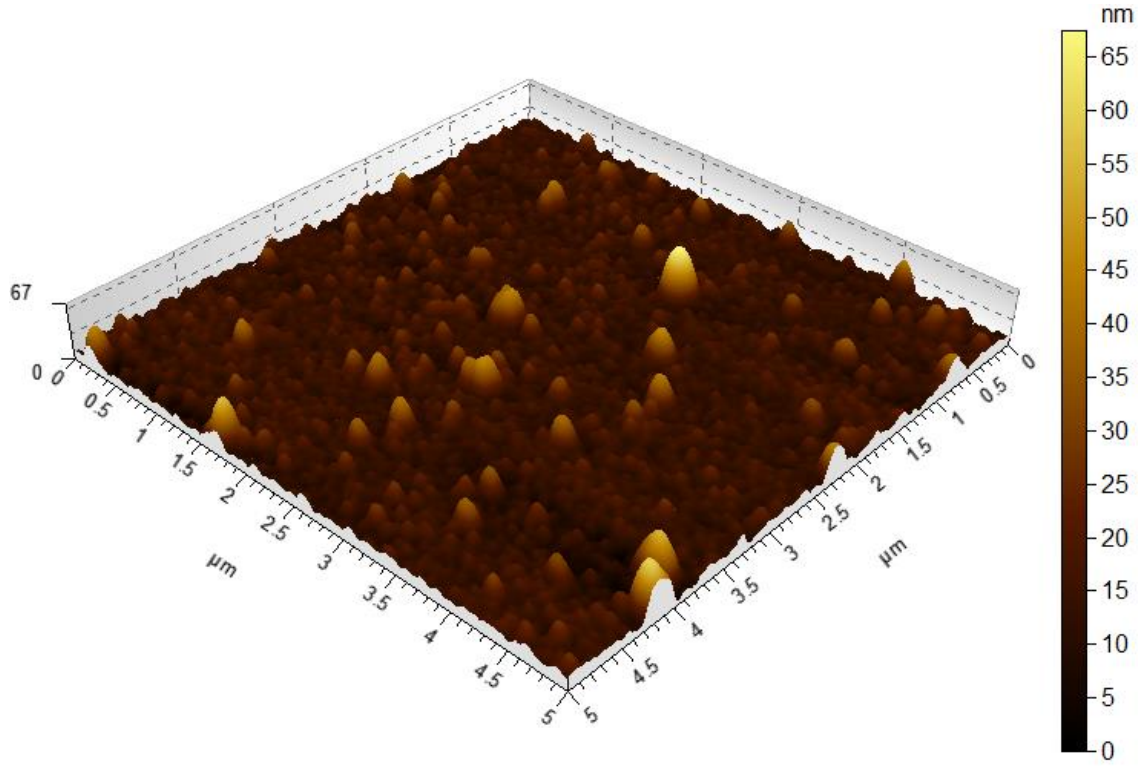

Figure 18 Atomic force microscope image of Al_2O_3/YSZ thin films grown at 300 K.

List of Tables

Table 1 Summary of characteristics of precursor powders and pellets used as coating targets in the present study

Parameters	**YSZ powder**	**YSZ pellet**	**Al_2O_3 powder**	**Al_2O_3 pellet**
Particle size, µm	15-85	-	22- 45	-
Phases and its percentage	m-ZrO_2 (29.1%) and t-ZrO_2 (70.9%)	m-ZrO_2 (2.6%) and t-ZrO_2 (97.4%)	α-Al_2O_3 (100%)	α-Al_2O_3 (100%)
Crystallite size, nm	31 (m-ZrO_2) and 31 (t-ZrO_2)	28 (m-ZrO_2) and 29 (t-ZrO_2)	~ 97	~ 120
Lattice strain (%)	0.37 (m-ZrO_2) and 0.30 (t-ZrO_2)	0.48 (m-ZrO_2) and 0.34 (t-ZrO_2)	~ 0.12	~ 0.08

Table 2 Residual stress developed on pulsed laser deposited YSZ films at different substrate temperature

Substrate temperature (K)	**Residual stress (GPa)**	
	σ_{11}	σ_{22}
573	-8.1	-6.4
773	-7.5	-5.5
973	-3.0	-1.7

CITATION

S. Nath, I. Manna, S.K. Ray and J. Dutta Majumdar, Development and Characterization of Yttria Stabilized Zirconia and Al_2O_3 Thin Films by Pulsed Laser Deposition, Lasers in Eng., Vol. 35, pp. 101–122.